HEFAT2011
8th International Conference on Heat Transfer, Fluid Mechanics and Thermodynamics
11 – 13 July 2011
Pointe Aux Piments, Mauritius

TURBULENT DISPERSION OF PARTICLES IN A DIFFERENTIALLY HEATED VERTICAL CHANNEL

J. Pallares* and F.X. Grau
*Author for correspondence
Department of Mechanical Engineering,
University Rovira i Virgili,
Av. Països Catalans, 26. 43007-Tarragona.,
Spain,
E-mail: jordi.pallares@urv.cat

ABSTRACT

Direct numerical simulations of particle dispersion in the turbulent natural convection flow between two vertical walls kept at constant but different temperatures are reported. It is assumed that the particles do not affect the flow (i.e. the dilute phase approximation is adopted). Particles with different levels of inertia or Stokes numbers ($0.843 \leq St \leq 17.45$) are tracked according to the drag force imposed by the fluid. The gravity force is also included for two cases, $St=0.843$ and $St=17.45$. The different level of turbulence near the wall and near the center of the channel produces, as in isothermal turbulent channel or pipe flow, a larger concentration of particles near the wall. This effect becomes more important, and the deposition velocity of particles on the wall increases, as the particle inertia is increased in a certain range of Stokes numbers ($0.843 \leq St \leq 8.38$). The simulations at $St=8.38$ and $St=17.45$ predict similar concentration profiles and deposition velocities according to the large inertia of these particles. For the conditions considered, the gravity vector imposes a strong descending motion on particles and this produces the increase of the particle concentration near the wall in comparison with the results without the gravity force.

INTRODUCTION

Flows that transport small particles, bubbles or drops can be found in many engineering, industrial and environmental situations. The determination of the rates and the mechanisms responsible for the dispersion and deposition on solid surfaces of the dispersed phase has been the topic of many studies because they have important implications in practical problems. Examples of such problems are the fouling of heat transfer equipment, aerosol deposition on surfaces or the transport and fallout of airborne pollutants. A considerable fraction of these numerical, theoretical and experimental studies have been devoted to the analysis of the particle dispersion in forced convection flows in pipes and channels. Excellent and extensive reviews of the topic can be found in [1] and [2].

The analyses of particulate flows in natural convection are scarce in the literature. The deposition of aerosol particles in laminar natural convection boundary layer was considered by Nazaroff and Cass [3] and Tsai [4] and by Akbar et al. [5] in laminar free convection in a square enclosure. The dispersion and deposition of aerosol and small particles in turbulent natural convection flows have implications, for example, in the air indoor quality and in the fouling of art pieces in museums and exhibitions [3]. The analysis of the behaviour of small particles in canonical turbulent natural convection flows has also a fundamental interest because it can help to determine the relative importance of the mechanisms responsible for the particle fluxes and the deposition rates on the walls.

In this study we analyze by direct numerical simulation (DNS) the particle dispersion and wall deposition produced by the turbulent natural convection flow between two vertical walls kept at different temperatures at low Rayleigh numbers [6-8]. The simulations were carried out using a Lagrangian particle tracking technique. As a first step and to determine the separated influence of the different forces that may act in the particles, we performed simulations with the aerodynamic drag force and simulations with the drag force and the gravitational force.

NOMENCLATURE

Ar	$Ar=g\,d_p^3(1-\rho_f/\rho_p)/\nu^2$	Arquimides number
C	[particles m^{-3}]	particle concentration
Cd		drag coefficient
d	[m]	diameter
g	[m s^{-2}]	gravitational acceleration
H		distance between the walls
J	[particles $m^{-2}\,s^{-1}$]	particle flux to the wall
l		distance to the wall
Pr	$Pr=\nu/\alpha$	Prandlt number,
Ra	$Ra=(g\beta\Delta TH^3)/(\nu\,\alpha)$	Rayleigh number,
St	$St=t_p/t_f=(d_p^2\rho_p/18\mu)/(\nu/u_\tau^2)$	Stokes number,
T	[K]	temperature
t	[s]	time
tf	$t_f=\nu/u_\tau^2$, [s],	characteristic time scale of the flow
tp	$t_p=(d_p^2\rho_p/18\,\mu)$, [s]	characteristic time scale of the particle
u,v,w	[m s^{-1}]	velocity components
u_τ	$u_\tau=(\langle\tau_w\rangle/\rho_f)^{1/2}$[m/s]	friction velocity,
V_d*	$V_d^*=J/(C_i\,u_\tau)$	non-dimensional deposition velocity
x, y, z	[m]	Cartesian coordinates
Greek letters		
Δ		increment
α	[$m^2\,s^{-1}$]	thermal diffusivity
β	[K^{-1}]	coefficient of thermal expansion
δ_{ij}		Kronecker's delta
μ	[Pa s]	dynamic viscosity
ν	[$m^2\,s^{-1}$]	kinematic viscosity
ρ	[kg m^{-3}]	density
τ	[Pa]	shear stress
Subscripts and superscripts		
f		fluid
c		cold
h		hot
i		initial
o		value at the temperature of reference
p		particle
w		wall
*		non-dimensional quantity

PHYSICAL MODEL

Figure 1 shows the coordinate system and the computational domain of the vertical channel. The natural convection flow, driven by the temperature difference imposed at the walls of the channel, is assumed to be hydrodynamically and thermally fully developed. The two walls of the channel located at $y=-H/2$ and $y=H/2$ are rigid, smooth and they are kept at constant but different temperatures. All physical properties of the fluid, with a Prandtl number ($Pr=\nu/\alpha$) of 0.7, are considered constant except for the linear variation of the density with temperature which is considered only in the buoyancy term according to the Boussinesq approximation. The viscous dissipation and the radiation heat transfer are neglected.

The particles are assumed to be spherical and the heat and/or mass transfer between the fluid and the particles are neglected. It is assumed that the particles do not affect the flow and the fluid properties. The forces considered acting in the particles are the hydrodynamic drag force and the gravity force. The pressure gradient force, the Basset force, the virtual mass force, the Brownian force, the Saffman's lift force and the thermophoretic force are neglected.

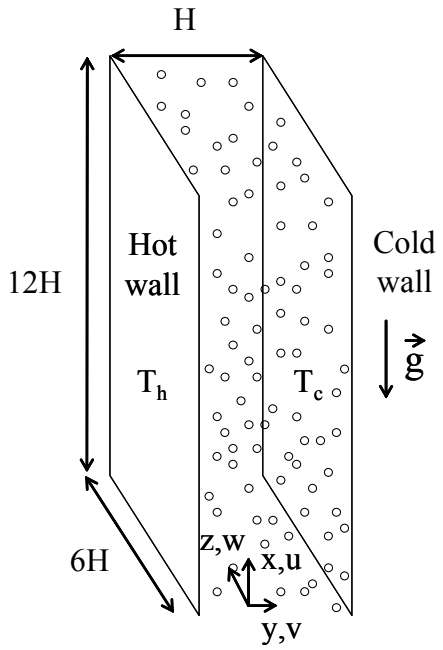

Figure 1 Physical model and coordinate system

MATHEMATICAL MODEL

The non-dimensional continuity, Navier-Stokes and thermal energy equations, that govern the momentum and thermal energy of the fluid, are

$$\frac{\partial u_i^*}{\partial x_i^*}=0 \tag{1}$$

$$\frac{\partial u_i^*}{\partial t^*}+\frac{\partial u_i^* u_j^*}{\partial x_j^*}=-\frac{\partial p^*}{\partial x_i^*}+Pr\frac{\partial^2 u_i^*}{\partial x_j^{*2}}+\delta_{i1}Ra\,Pr\,T^* \tag{2}$$

and

$$\frac{\partial T^*}{\partial t^*}+\frac{\partial u_i^* T^*}{\partial x_i^*}=\frac{\partial^2 T^*}{\partial x_i^{*2}}, \tag{3}$$

respectively.

The scales used to obtain the non-dimensional variables are the channel width (H) and the thermal diffusion time (H^2/α). The non-dimensional temperature is defined as $T^*=(T-T_o)/(T_h-T_c)$ where T_h and T_c are the temperatures of the hot and cold wall, respectively, $T_o=(T_h+T_c)/2$ is the mean temperature and $\Delta T=T_h-T_c$ is the temperature increment. The last term on the right-hand side of Eq. (2) corresponds to the non-dimensional buoyancy acceleration along the x-direction. In Eq. (2) Ra is the Rayleigh number, which has been set to $5.4\cdot10^5$. Periodic boundary conditions for velocities and temperature are applied along the x and z directions. The non-slip condition is imposed at the walls. The thermal boundary conditions are $T^*=0.5$ and $T^*=-0.5$ at the hot and cold wall, respectively.

Under the hypotheses indicated above, the position and the velocity of the particles are governed by

$$\frac{d\left(x_p^*\right)_i}{dt^*} = \left(u_p^*\right)_i \tag{4}$$

$$\frac{d\left(u_p^*\right)_i}{dt^*} = -\frac{3}{4}\frac{\rho_{fp}^*}{d_p^*} C_d \left|u_p^* - u^*\right| \left[\left(u_p^*\right)_i - \left(u^*\right)_i\right] - \frac{Ar\, Pr^2}{d_p^{*3}} \delta_{i1} \tag{5}$$

The first term on the right hand side of Eq. (5) is the hydrodynamic drag force and the second is the effective gravitational force which is proportional to the Archimides number, Ar. The drag coefficient is computed as [9]

$$C_d = \frac{24}{Re_p}\left(1 + 0.15\, Re_p^{0.687}\right) \tag{6}$$

and the particle Reynolds number is

$$Re_p = \frac{d_p \left|u_p - u\right|}{\nu} = \frac{d_p^* \left|u_p^* - u^*\right|}{Pr} \tag{7}$$

Equation (6) is valid for Re_p<800 [1]

The governing transport equations for the fluid, Eqs. 1 to 3, together with the boundary conditions are solved numerically with the 3DINAMICS code. This second-order accuracy finite volume code uses central differencing of the diffusive and convective terms on a staggered grid and a Crank-Nicolson scheme for the temporal discretization. The Poisson equation resulting from the coupling between the velocity and pressure fields is solved with an efficient parallel multigrid solver. More details about the code can be found in Fabregat [10].

The computational domain, with dimensions L_x=12.5·H, L_y=H, L_z=6.3·H, is divided into 121x100x121 grid nodes. They are uniformly distributed along the streamwise and spanwise homogeneous directions (Δx≈0.1·H and Δz≈0.05·H) in which periodic boundary conditions are imposed, while hyperbolic tangent distributions are used to stretch the nodes near the walls (Δy_{min}≈1.7·10^{-3}·H and Δy_{max}≈2.2·10^{-2}·H) where the no-slip condition is applied. The time step used to integrate numerically the transport equations is Δt=5·10^{-5}·H^2/α. The validation of the simulation of the flow can be found in Pallares et al. [8].

To track the particles, the velocities of the fluid are computed in an Eulerian grid using the 3DINAMICS code and they are interpolated to the positions of the particle using fourth order Lagrange polynomials. Initially, 10^5 particles are distributed randomly in the computational domain and their positions and velocities are calculated using Equations (4) and (5) which are integrated in time with a fourth order Runge-Kutta method with the same time step as for the time marching of the equations for the fluid. The particles that leave the computational domain through the periodic boundaries are reintroduced accordingly. Perfectly-elastic collisions are assumed when the particle center is at a distance from the wall lower than the particle radius.

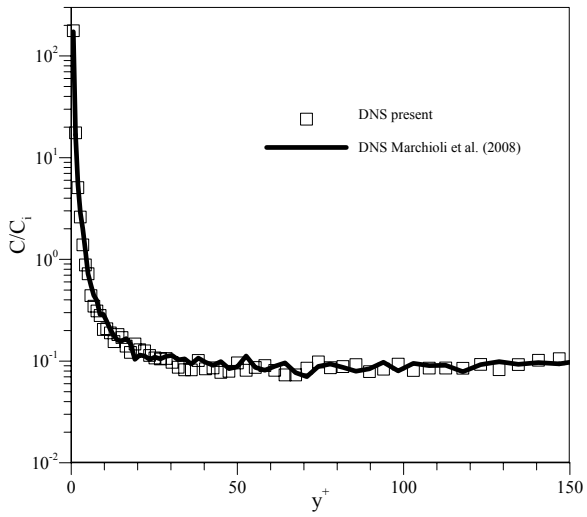

Figure 2 Time averaged particle concentration profile in turbulent plane channel flow. The concentration is scaled with the initial concentration of particles, C_i. The horizontal axis is the distance, l, to the wall of the channel in wall coordinates $y^+=u_\tau l/\nu$

The particle tracking method has been validated by simulating the dispersion of 10^5 particles in a plane turbulent channel flow for which results can be found in the literature. Particularly, we simulated the flow at a Reynolds number, based on the friction velocity (u_τ) and the channel half width, of Re_τ=150 and particles with a Stokes number of $St=\rho_p \cdot d_p^2 \cdot \rho_f u_\tau^2/(18\cdot\mu^2)$=25. The time averaged velocities and turbulence statistics of the fluid and the particles were in good agreement with those reported in Marchioli et al. [11] but they are not shown here for sake of brevity. As an example, Figure 2 shows that the time averaged concentration distribution for the flow condition considered is well reproduced using the present particle tracking method.

RESULTS AND DISCUSSION

Table 1 shows the different sizes of the particles and the non-dimensional parameters considered for the simulations. A possible set of dimensional parameters that corresponds to the non-dimensional values of Table 1 is indicated in Table 2. It can be seen in Table 1 that two simulations considering the gravitational force [$Ar\neq0$] are reported and they correspond to the smallest and to largest particles for Ar=0.

Ra	Pr	ρ_{fp}^*	St	dp^*	Ar	$ArPr^2/dp^{*3}$
5.4 10^5	0.7	1.30·10^{-3}	0.843	1.11 10^{-3}	0	0
					0.0158	5.66 10^6
			1.75	1.60 10^{-3}	0	0
			8.38	3.50 10^{-3}	0	0
			17.45	5.05 10^{-3}	0	0
					1.49	5.66 10^6

Table 1 Non-dimensional parameters

g [m s^{-2}]	ρ_f [kg m^{-3}]	μ [Pa s]	β [K^{-1}]	α [m s^{-2}]	H [m]	ρ_p [kg m^{-3}]	ΔT [K]
9.81	1.3	$2.05\cdot10^{-5}$	$3.33\cdot10^{-3}$	$2.24\cdot10^{-5}$	0.0662	1000	20

d_p [m]
$7.35\ 10^{-5}\leq d_p\leq 3.35\ 10^{-4}$

Table 2 Dimensional parameters. The physical properties of the fluid correspond to air at ambient pressure and temperature

Particle concentrations

The particle statistics were computed by averaging over wall-parallel slabs with the same thicknesses as the sizes of the control volumes used for the discretization of Eqs. [1-3] along the y-direction. The thicknesses of the slabs near the walls of the channel were set equal to the diameter of the particle. As an example, Figure 3 shows the time evolution of the non-dimensional concentration of particles, for Ar=0, in the central slab, centered at y^*=0, and in the third slab near the hot wall, centered at y^*=-0.493. It can be seen that the uniform initial particle distribution (C/C_i =1) progressively evolves towards a particle distribution with a higher concentration of particles near the wall than in the center of the channel. This phenomenon, often refereed as "turbophoresis" [1], is produced by the larger turbulence intensity far from the walls than near the wall region. Note that for the data plotted in Figure 3, the only force that act on the particles is the hydrodynamic drag force (i.e. Ar=0). The accumulation of particles near the walls indicates that the particle fluxes towards the wall are more efficient than the particle fluxes away from the wall. As shown in Figure 3 the steady state is reached for t^*>0.2 for all the sizes of the particles. Typically, the simulations were run until $t^*\approx$2.

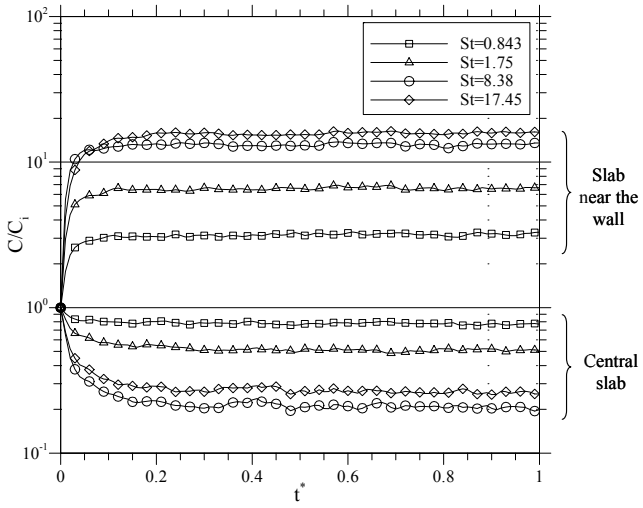

Figure 3 Time evolution of the particle concentration in the central slab and in a slab near the wall for Ar=0

The profiles of the time-averaged concentration of particles for Ar=0 when the distributions of particles are statistically steady, are shown in Figure 4. The concentration in each slab was averaged during 1.5 non-dimensional time units and because of symmetry at Ar=0 the profiles were further averaged with respect to y^*=0.

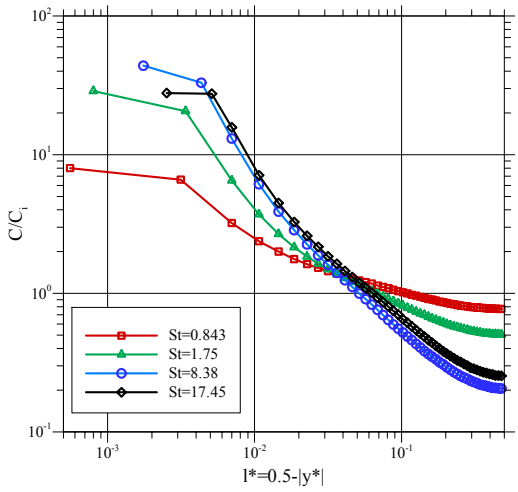

Figure 4 Time-averaged concentration profiles at Ar=0

Figure 4 shows that the time-averaged concentration near the wall increases as the diameter of the particle increases except for the largest particle considered (St=17.45) for which the concentration at the slab nearest to the wall is smaller than that of the particles with St=8.38. It can be seen that the concentration near the center of the channel decreases as the particle diameter increases from St=0.843 to St=8.38 and it increases from St=8.38 to St=17.45. The same trend was observed by Marchioli et al. [12] in their DNS of particle dispersion in the isothermal turbulent flow in a vertical pipe.

According to the experimental and theoretical results available in the literature [13], the deposition velocities of particles on the walls of isothermal vertical turbulent channel and pipe flows can be divided into three regimes depending on the size of the particles, or the Stokes number of the particle. Figure 5 shows the non-dimensional deposition velocity for different Stokes numbers. Although the three regimes are not clearly separated by critical values of the Stokes number, (i.e. the borders between the different regimes are not sharp) each regime has its dominant mechanism for the particle deposition on the wall. The first regime, typical of very small particles with St<0.3, that follow very well the fluid velocity, is known as the turbulent diffusion regime and the particle transport to the wall is well represented by a gradient turbulent diffusion model. The deposition velocity slightly decreases as the Stokes number increases. The second regime (0.3<St<20) is the diffusion-impaction regime and the dominant deposition mechanism is well represented by the result of the interaction of the non-negligible particle inertia and the fluid turbulent eddies. It can be seen in Figure 5 that in this regime the deposition velocity increases by about three orders of magnitude. The third regime is known as the inertia-moderated regime (St>20) and correspond to very massive particles that acquire sufficient momentum from the large eddies of the core to reach the wall directly. In this regime the deposition velocity slightly decreases with the Stokes number. It should be

emphasized that these values of the Stokes numbers are valid for isothermal flow in vertical channels or pipes.

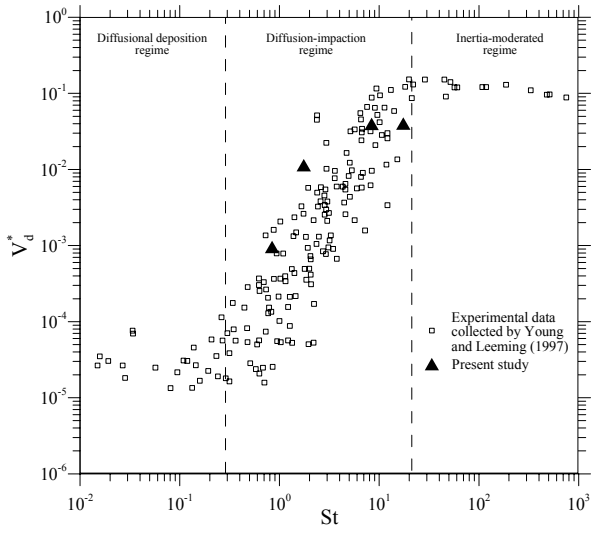

Figure 5 Deposition velocities vs. Stokes number

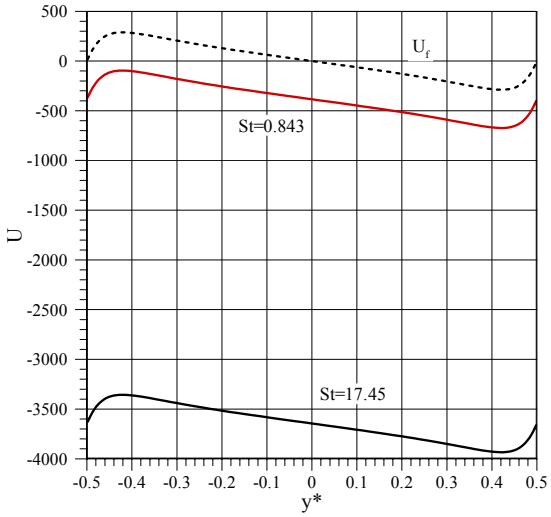

Figure 6 Time-averaged vertical velocities of the fluid and of particles with St=0.843 and St=17.45

In Figure 5 we plotted the deposition velocity for the natural convection flow considered in this study for the cases at Ar=0. The deposition velocity was computed counting the number of different particles that reach the walls during about 0.3 non-dimensional time units when the distribution of particles was statistically in steady-state. It can be seen in Figure 5 that the trend of the present predictions of V_d^* reproduce the trend corresponding to the isothermal flows but the data is shifted to lower Stokes numbers and lower deposition velocities. Figure 5 shows that according to the variation of the deposition velocity with the Stokes number described above for isothermal flows, the present results at $0.843 \leq St \leq 8.38$, predict an increase of the deposition velocity, typical of the diffusion-impaction regime. On the other hand the deposition velocity slightly decrease increasing the Stokes number from St=8.38 to St=17.45. This is the trend of the inertia moderated regime, as shown in Figure 5. These trends suggest that the results at $St<8.38$ correspond to the diffusion-impaction regime and the results at $St \geq 8.38$ to the inertia moderated regime. This classification supports the observed differences of the profiles of the time-averaged concentration (see Fig. 4). In this figure the profiles corresponding to St=8.38 and St=17.45 are similar while the profiles at St=0.843 and St=1.75 show a substantial different level of uniformity in the concentration distribution. In addition the larger deposition velocity at St=8.38 than at St=17.45 (see Fig. 5) agrees with the larger concentration of particles at St=8.38 than at St=17.45, shown in Figure 4.

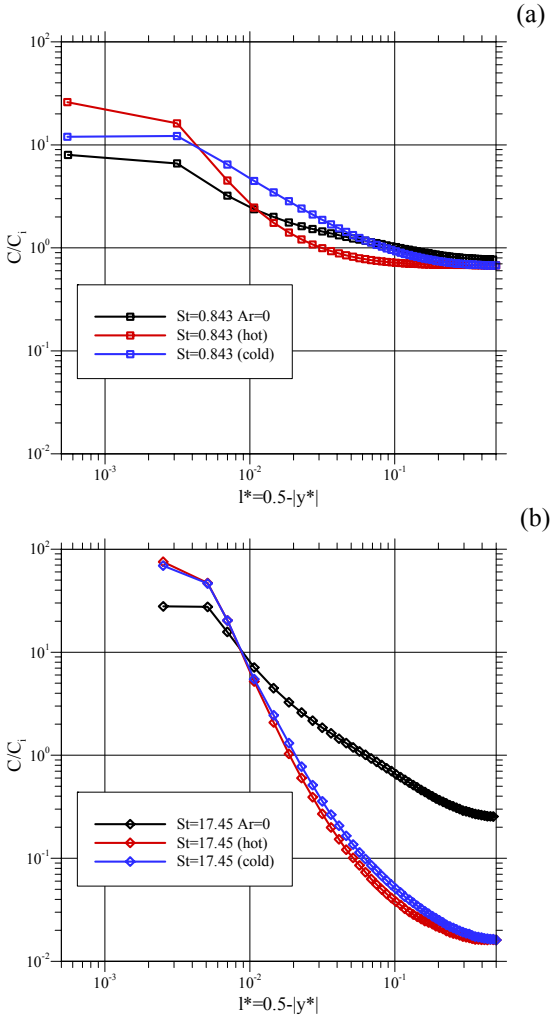

Figure 7 Time-averaged concentration profiles at (a) St=0.845 and (b) St=17.45 at Ar=0 (black lines) and at $Ar \neq 0$. Red lines correspond to the region near the hot wall ($0>y^*>-0.5$) and blue lines to the region near the cold wall

We simulated two cases considering the combined effect of the drag force and the gravitational force (see Table 1). Figure 6 shows the time-averaged fluid and particle velocities for St=0.843 and St=17.45. It can be seen that because of gravity the particles with different sizes fall with different terminal velocities. The averaged terminal velocities are $-385\alpha/H$ and

-3650 α/H for St=0.843 and St=17.45, respectively. The absolute values of these velocities are larger than the maximum averaged velocity of the fluid, which is 289 α/H (see Fig. 6).

The time averaged profiles of concentrations at St=0.843 and St=17.45 for Ar≠0 are shown in Figures 7.a and 7.b, respectively. The profiles corresponding profiles at Ar=0 are also included for comparison. It can be seen that the gravity force produces larger concentrations of particles near the cold wall than in the region near the hot wall, especially for the smaller particles (Fig. 7.a). This tendency is reversed very near the wall, as shown in Figure 7.a, where the concentration of particles for $l^*<4\cdot10^{-3}$ is larger near the hot wall than near the cold wall. It is noticeable the dramatic reduction of the concentration of particles near the center of the channel and the corresponding increase of concentration near the wall in the case of St=17.45 and Ar≠0 with respect to the case with Ar=0, as shown in Figure 7.b.

Fluctuation intensities

The time-averaged distributions of particles shown in Figures 4 and 7 are direct consequences of the fluctuation intensities of the velocity component perpendicular to the wall that transport the particles from the center of the channel towards the walls with a larger probability (or efficiency) than from the walls towards the center of the channel until a steady state is reached.

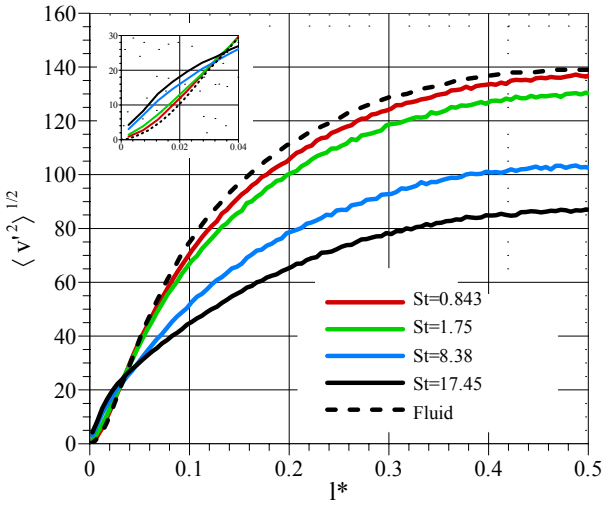

Figure 8 Fluctuation intensities of the velocity component perpendicular to the wall of the fluid and of the particles for Ar=0 as a function of the distance to the wall (l^*=0.5 -|y^*|). The inset shows an enlargement of the near-wall region.

Figure 8 shows the fluctuation intensity of the velocity component perpendicular to the wall for the fluid and for the particles with Ar=0. It can be seen that near the center of the channel (l^*=0.5) the particles with low inertia have a similar distribution of the fluctuation intensities of that of the fluid while the large particles (St=17.45) have a lower intensities according with their larger inertia. Note that the relatively small differences in the fluctuation intensities of the smallest particles considered (St=0.843) and those of the fluid (see Fig. 8) produce a significant deviation of the uniform concentration distribution (C/C_i = 1) that would be obtained if the particles would follow perfectly the velocity field of the fluid (i.e. for particles without inertia with $(u_p)_i=(u_f)_i$). For example, it can be seen in Figure 4 that at St=0.843 the concentration of particles is 0.77 in the center of the channel and 8.0 near the wall.

It can be seen in Figure 8 that, near the wall (l^*<0.04), the fluctuation intensities of the particles are larger than those of the fluid, especially for the larger particles. This is in agreement with the fact the large particles, with large inertia reach the wall with a large velocity that the particle has acquired farther from the wall.

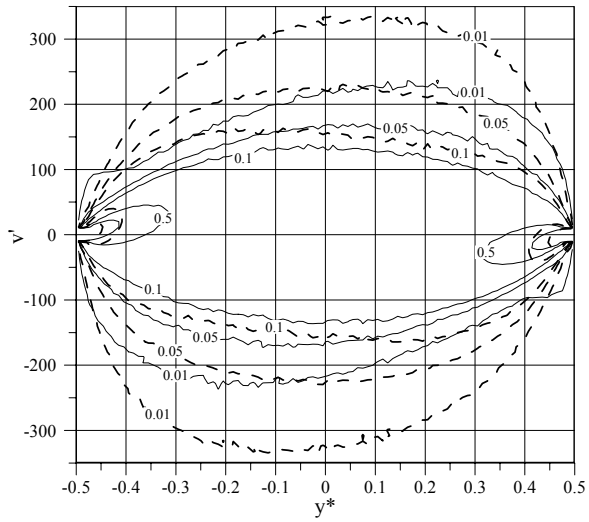

Figure 9 Joint probability density function of the fluctuations of the velocity component perpendicular to the wall for St=0.843 (dashed line contours) and St=17.45 (continuous line contours) for Ar=0 as a function of y^*

To clarify this point Figure 9 shows the joint probability density function of the velocity fluctuation perpendicular to the wall as a function of the normal-to-the-wall coordinate, y*, for St=0.843 and St=17.45, at Ar=0. Note that by definition $\int_{-\infty}^{\infty}\left(\int_{-0.5}^{0.5} PDF\, dy^*\right)dv' = 1$. It can be seen that the fluctuations are not symmetrically distributed with respect to v'=0. Near the hot wall (for example at y^*=-0.3) the positive fluctuations (v'>0) that transport particles away form the wall are more probable (about 60%) than the negative fluctuations (v'>0) that transport particles towards the wall (about 40%). These proportions are approximately valid for the two sets of particles, St=0.843 and St=17.45, shown in Figure 9. Although the velocity fluctuations away from the walls are more probable than the fluctuations towards the walls, the fluctuations towards the walls have larger probabilities at larger intensities. For example, near the hot wall, at y^*=-0.3 and v'=-200 the values of the PDFs for St=0.843 and St=17.45 are 0.04 and 0.01, respectively, but at y^*=-0.3 and v'=200 they are 0.03 for St=0.843 and approximately zero for St=17.45. This indicates that, on average, at the steady state, there is a large number of

particles that leave the near-wall region at low velocities and there is a small number of particles that enter the near-wall region at large velocities. This mechanism is more important as the inertia of the particle is increased as illustrated in Figure 9, where it is seen that the PDF of the particles with St=0.843 is more symmetric with respect to v'=0 than the PDF of the particles with St=17.45.

It is remarkable the relative large increase of the velocity fluctuations away from the wall in the near-wall region (at $|y^*|>0.475$) if one compares the PDF of St=17.45 with that of St=0.843. This increase can be attributed to the perfectly-elastic collision adopted when a particle reach the wall. In this case, at St=17.45 some of the particles reach the wall with a large impact velocity and rebound with that velocity away from the wall.

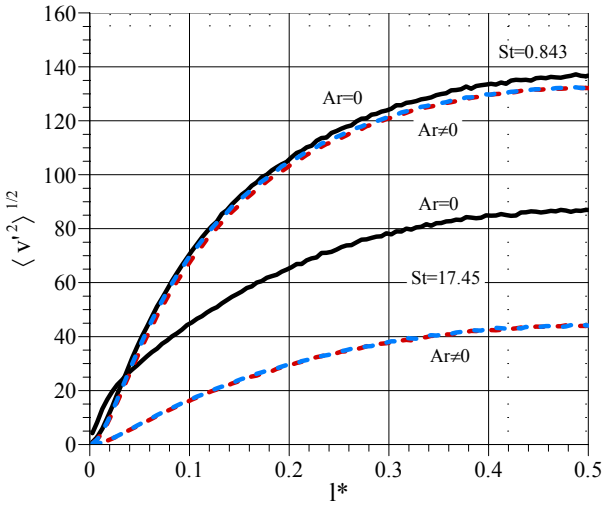

Figure 10 Fluctuation intensities of the velocity component of the particles perpendicular to the wall for Ar=0 (black continuous lines) and for Ar≠0 (dashed line). The red/blue color of the profiles for Ar≠0 corresponds to the hot/cold near wall region

The effect of the gravity vector on the profiles of the fluctuation intensities of the velocity component perpendicular to the wall is shown in Figure 10. It can be seen that for the large particles, at Ar≠0 there is an important reduction of the fluctuation intensities in comparison with Ar=0. This reduction is also observed in the vertical fluctuation intensities, $\langle u'^2 \rangle$, not shown here for sake of brevity. For the conditions considered at Ar≠0 the relatively strong vertical descending motion imposed by the gravity vector (see Fig. 6) produces that the particles become more insensitive to the fluctuations of the fluid velocity. Under these conditions, the fluctuations of the fluid velocity that transport particles away from the near wall region are more ineffective because the particles near the wall have an important descending velocity (see Fig. 6). This effect produces the increase of the particle concentration near the walls for Ar≠0 in comparison with Ar=0, as shown in Figure 7.

CONCLUSION

The preferential concentration of particles in a turbulent natural convection vertical channel flow has been analyzed. Particles with different inertia are accumulated differently in the near wall region of the flow. It has been found that, for the conditions considered, as the Stokes number increases in the range $0.843 \le St \le 8.38$ there is a progressive increase of the concentration of particles near the wall as well as of the deposition velocity of particles on the wall. In the range $St \ge 8.38$, which correspond to particles with a very large inertia, the concentration of particles near the wall and the deposition velocity slightly decreases. The probability density function of the fluctuations of the velocity component perpendicular to the wall shows that near the walls the velocity fluctuations away from the wall are more probable than the velocity fluctuations towards the wall. However, the velocity fluctuations away from the wall have less intensity than the velocity fluctuations towards the wall. This produces that particles with large inertia are effectively accumulated in the near wall region, until a statistically steady state is reached. The gravitational acceleration, for the particles considered, imposes an important descending motion to the particles and it reduces considerably the intensity of the fluctuations of velocity, specially for the large particles. This reduction increases the accumulation of particles near the wall in comparison with the conditions without gravity.

REFERENCES

[1] Michaelides, E. E. "Particles, bubbles and drops – Their motion, heat and mass transfer" World Scientific Publishing, Singapore, 2006

[2] Guha, A. Transport and deposition of particles in turbulent and laminar flow, *Annual Review of Fluid Mechanics*, Vol. 40, 2008, pp. 311-341

[3] Nazaroff W., and Cass G. R., Particle deposition from a natural convection flow onto a vertical isothermal flat plate, *Journal of Aerosol Science,* Vol. 18, No. 4, 1987, pp. 445-455

[4] Tsai R., Aerosol particle transport in a natural convection flow onto a vertical flat plate, *International Journal of Heat and Mass Transfer*, Vol. 44, 2001, pp. 867-870

[5] Akbar, M. K., Rahman, M., Ghiaasiaan, S. M., Particle transport in a small square enclosure in laminar natural convection, *Aerosol Science*, Vol. 40, 2009, pp. 747-761

[6] Versteegh T. A. M and Nieuwstadt F. T. M, Turbulent budgets of natural convection in an infinite, differentially heated, vertical channel. *International Journal of Heat and Fluid Flow,* Vol. 19, 1998, pp. 135-149

[7] Versteegh T. A. M. and Nieuwstadt F. T. M., A direct numerical simulation of natural convection between two infinite vertical differentially heated walls: scaling laws and wall functions. *International Journal of Heat and Mass Transfer,* Vol. 42, 1999, pp. 3673-3693

[8] Pallares J., Vernet A., Ferre J. A. and Grau F. X., Turbulent large-scale structures in natural convection vertical channel flow, *International Journal of Heat and Mass Transfer,* Vol. 53, 2010, pp. 4168-4175

[9] Schiller, L. and Nauman, A., 1933, "Uber die grundlegende Berechnung bei der Schwekraftaufbereitung," *Ver. Deutch Ing.,* 44, pp. 318-320.
[10] Fabregat, A. Direct numerical simulation of turbulent dispersion of buoyant plumes in a pressure-driven channel flow, Ph.D. Thesis, Department of Mechanical Engineering, University Rovira i Virgili; Tarragona, Spain, 2006.
[11] Marchioli C., Soldati A., Kuerten J. G. M, Arcen B., Tanière B., Goldensoph G., Squires K. D., Cargnelutti M. F. and Portela L. M. Statistics of particle dispersion in direct numerical simulations of wall-bounded turbulence: Results of an international collaborative benchmark test, *International Journal of Multiphase Flow*, Vol. 34, 2008, pp. 879-893
[12] Marchioli C., Giusti A., Salvetti M. V. and Soldati A., Direct numerical simulation of particle wall transfer and deposition in upward turbulent pipe flow, *International Journal of Multiphase Flow*, Vol. 29, 2003, pp. 1017-1038
[13] Young J., and Leeming A., A theory of particle deposition in turbulent pipe flow, *Journal of Fluid Mechanics*, Vol. 340, 1997, pp. 129-159